Categorization of tars from fast pyrolysis of pure lignocellulosic compounds at high temperature

Anna Trubetskaya[a,*], Nabil Souihi[b,**], Kentaro Umeki[c,]

[a]*School of Engineering and Ryan Institute, National University of Ireland Galway, Galway, Ireland*
[b]*Green Technologies and Environmental Economics Platform, Department of Chemistry, Umeå University, 90187, Umeå, Sweden*
[c]*Division of Energy Science, Luleå University of Technology, 97187, Luleå, Sweden*

Abstract

This study presents how the yields of different tar compounds from pure lignocellulosic compound respond to the change in temperature and residence time. Experiments were carried out with a drop tube furnace in the temperature range from 800 to 1250°C. The tar composition was characterized by gas chromatography with a flame ionization detector and mass spectrometry using a dual detector system. Longer residence time and higher heat treatment temperatures increased the soot formation and decreased the tar yields. Soot yields from lignin samples were greater than soot yields from holocellulose pyrolysis. The dominating products in tars from pyrolysis of all lignocellulosic compounds were benzene and toluene. Cellulose and hemicellulose pyrolysis produced greater amount of oxygenates in tars, whereas lignin tar was rich in phenols, polycyclic hydrocarbons and naphthalenes. Simultaneous reduction of tar and soot was achieved by impregnation of lignin

*Corresponding author. anna.trubetskaya@nuigalway.ie
**Corresponding author. nabil.souihi@umu.se
Corresponding author. kentaro.umeki@ltu.se

from wheat straw with alkali metals. The OPLS-DA model can accurately explain the differences in tar composition based on the experimental mass spectrometry data.
Keywords: fast pyrolysis, lignocellulosic compounds, potassium, tar, principal component analysis

1. Introduction

Lignocellulosic biomass has a potential to replace fossil fuels in the production of liquid hydrocarbons and chemicals [1]. Biomass gasification offers high conversion efficiency and the possibility to handle different lignocelluloses [2]. Owing to the high volatile content in biomass, a major challenge in biomass gasification is usually tar content in syngas, which decreases the cold gas efficiency and requires cost-intensive cleaning systems. Entrained flow gasification (EFG) process generates little or no tar due to high operating temperatures although it produces considerable amount of soot.

In order to reduce the soot yield from EFG process it is necessary to understand how tar composition and yield are correlated with fuel composition and operating conditions since soot is formed as a result of the reactions between PAHs. Tars are defined as a complex mixture of hydrocarbons with single or multiple rings [3]. Primary tars are generated during devolatilization at the temperatures of 400-500°C, followed by a series of cracking reactions [4]. Primary tars are predominantly oxygenated organic compounds similar to the original structures of lignocellulosic compounds. Primary tars from cellulose and hemicellulose are levoglucosan, xylose and non-aromatic oxygenated compounds (ketones, aldehydes, and alcohols) while primary tars from lignin

contain mainly phenolic compounds [5–7]. Secondary reactions take place both heterogeneously and homogeneously, and include intra-particle cracking of tar on the char surfaces [4, 8]. The secondary tars are mainly composed of phenols and olefins [9]. The tertiary products are generated above 700°C and subdivided into alkyl aromatics and larger polycyclic aromatic hydrocarbons e.g. benzene, toluene, naphthalene, pyrene, etc. [10–12]. The molecular structure of tertiary tars cannot be found in natural biomass and can emerge from small molecule fragments as allyl-, aryl-, and alkyl radicals, which result from cycloaddition reactions according to Diels-Alder and followed by aromatization due to dehydrogenation respectively dehydration [9]. As well known from a number of studies on the combustion of gaseous and liquid fuel combustion [13], polycyclic aromatic hydrocarbons (PAH) are thought to be the main precursors of soot [14, 15]. Some studies suggested to represent tar with two lumped compounds of primary tar (acetol and catechol) [6, 16] or by three lumped compounds (acetol, toluene) [5]. Palma et al. [6] suggested that the most abundant tar compounds in wood gasification were catechol, *o*-cresol and salicylaldehyde from lignin. The kinetic model of Jess [17] showed that benzene is the key component of thermal decomposition of aromatic hydrocarbons, and naphthalene is a precursor of soot formation. In order to reduce the yield of soot during gasification, it is necessary to understand how tar composition and yield are correlated with fuel composition and operating conditions.

The formation of tars depends strongly on the operational conditions of gasification [18]. A number of studies investigated the effect of heating rate, temperature and pressure on the yields and composition of primary tar under

fast pyrolysis conditions. The large particle sizes and increasing pressure led to the tar yield decrease in wood and cellulose pyrolysis [8, 19]. Furthermore, the yields and average molecular weight of tars from pyrolysis of cellulose, lignin and pinewood decreased with lowering heating rates and increasing alkali content (potassium and sodium) [20, 21]. The proportion of heavier tars in pinewood pyrolysis increased with the higher temperatures and longer residence time due to the enhanced polymerization reactions between aromatic tar compounds to form larger PAHs [22].

Despite of numerous previous studies on fast pyrolysis of various feedstocks at high temperatures [22–25], few studies, have systematically investigated how the chemical and structural variance of biomass affects the tar yield and composition. It is difficult to identify how the tar yield and composition are affected by the origin of the feedstock. Therefore, a basic study of fast pyrolysis using major biomass components is important, and beneficial for the optimization of industrial processes such as entrained-flow gasifiers. The specific objectives of this study were: (1) to obtain knowledge about lignin type (softwood and wheat straw), and holocelluloses influence on the tar and soot yields during high-temperature fast pyrolysis, (2) to relate the product distribution of tar compounds to the soot yields at different residence times and temperatures, and (3) to quantify as many components of tar samples as possible using GC-FID and GC-MS techniques.

2. Materials and methods

The effects of lignocellulosic compounds and potassium on the product yields and composition were investigated in the drop tube reactor as de-

scribed previously [26]. Two types of organosolv lignin made from softwood and wheat straw (purity > 94 %) were provided by BOC Sciences. Cellulose Avicel® (purity > 99.9 %) and xylan from beechwood (purity > 90 %) were supplied by Sigma-Aldrich. The purity of xylan was additionally improved from 90 % to 96.6 % by a three step procedure involving a strong alkali treatment, bleaching and acetylation. The effect of potassium on the product yield and composition was investigated by wheat straw lignin impregnation with potassium nitrate. The lignocellulosic compounds were reacted in the drop tube reactor (DTF) at temperatures of 800-1250°C. The quantitative analysis of tar compounds which were identified by GC-MS was performed using GC-FID. The response factors for the known tar compounds were determined.

2.1. Original fuel characterization

The ultimate and proximate analysis of the lignocellulosic compounds was carried out at University of Agder, Department of Science and Engineering and shown in Table 1.

Table 1: Proximate, ultimate and ash analyses of cellulose, xylan from beechwood (hemicellulose), lignin from softwood and lignin from wheat straw.

	Cellulose	Xylan from beechwood	Lignin from softwood	Lignin from wheat straw
Proximate and ultimate analysis (% on dry basis)				
Moisture[a]	6	6	4.1	3.8
Ash (550 °C)	0.3	3.7	1.3	3.6
Volatiles	94.9	81.6	67.3	66.3
HHV[b]	18	14	26.4	26.7
LHV[b]	16.1	12.2	24.9	25.2
C	42.3	39.6	59.9	61.1
H	6.3	6	5.5	5.6
O	50.9	52.3	31.9	28.2
N	0.3	0.2	1.2	0.8

[a] wt. % (as received) [b] in MJ kg^{-1}

The ash content of lignocellulosic compounds was determined using a standard ash test at 550°C, according to the procedure described in DIN EN 14775. Lignin from wheat straw was rich in Na, Si and Fe (Na: 0.7 wt.% of the dry material; Si: 0.4 wt.% of the dry material; Fe: 0.1 wt.% of the dry material), whereas lignin from softwood contained a smaller fraction of Na (0.4 wt.% of the dry material). Xylan from beechwood after purification contained low amounts of Na and Ca (Na: 2 wt.% of the dry material; Ca: 0.6 wt.% of the dry material), as shown in supplementary Table S-1. The effect of potassium on the product yield and composition was investigated by wheat straw impregnation with potassium nitrate (Alfa Aesar, purity $> 99\,\%$), which was diluted in deionized water and added to 50 mg lignin. The impregnated lignin had a similar potassium content to the wheat straw (1.9 %, db) [27]. The addition of alkali nitrates did not affect the carbon balance compared to the impregnation with alkali carbonates, and nitrates

can be easily decomposed by a simple increase of temperature [28].

2.1.1. ^{13}C solid state NMR spectroscopy

Solid-state NMR analysis was carried out on a Bruker Avance 400 NMR spectrometer (9.4 T) operating at Larmor frequencies of 400.13, 100.58 and 79.48 MHz for ^{1}H and ^{13}C respectively. All experiments were conducted using a double resonance probe equipped with 4 mm (o.d.) rotors. Samples were analyzed at room temperature by single-pulse (SP) magic angle spinning (MAS) as well as cross polarization (CP) MAS [29] utilizing high-power ^{1}H two-pulse phase-modulated decoupling (TPPM) [30] during acquisition and employing a spin-rate of 9 kHz. The ^{13}C CP/MAS spectra were recorded using a recycle delay of 8 s, a contact time of 1 ms, an acquisition time of 45.9 ms and 4096 scans, whereas the ^{13}C SP/MAS spectra were recorded using a recycle delay of 128 s, an acquisition time of 45.9 ms and 1080 scans. All ^{13}C NMR spectra were referenced to the carbonyl resonance of an external sample of α-glycine at 176.5 ppm.

2.1.2. FTIR Spectroscopy

The lignin samples were analyzed by a Thermo Nicolet 6700 FTIR spectrometer equipped with a Golden gate (diamond) ATR accessory and DTGS (KBr) detector. All absorbance spectra were obtained in the 4000-600 cm^{-1} range by 100 scans at 4 cm^{-1} resolution. For background, 200 scans were acquired. A good contact between sample and ATR-crystal surface was ensured by the pressure device of the unit (up to 30000 psi) [31]. All samples were measured in triplicate.

2.2. Fast pyrolysis in drop tube reactor

The lignocellulosic compounds were reacted at three particle residence times (800°C: 0.12, 0.25, 0.5 s; 1000°C: 0.1, 0.2, 0.42 s; 1250°C: 0.09, 0.17, 0.35 s) in a laminar drop tube reactor. The DTF setup was described in detail by Trubetskaya et al. [26]. The residence time was varied by using different reactor lengths (0.72, 1.06 and 2.12 m), while the flow rate of feed gases was kept constant. Reaction products were separated into coarse particles (mainly char and fly ashes), fine particles (mainly soot and ash aerosols), permanent gases, and tars. Soot particles passing the cyclone (cut size 2.5μm) were captured from the product gas flow by a grade QM-A quartz filter with a diameter of 50 mm (Whatman, GE Healthcare Life Science). The tars from the product gas flow were collected in three serially connected gas washing bottles, each of which was filled with 30 ml of methanol (HiPerSolv CHROMANORM®, purity > 99.8 %). The temperature of methanol was kept at -50°C by the cooling bath Proline Edition X (LAUDA Dr. R. Wobser GmbH, Germany).

2.3. Tar analysis

For the semiquantification of annotated substances, 5 μl of an internal standard (Chlorobenzene, Sigma-Aldrich) was injected in the whole volume of tars dissolved in methanol. Prior to the GC-FID analysis, a 1.5 ml aliquot was pipetted into the autosampler screw cap vial and stored in the freezer at -20°C. The quantitative analysis of tar compounds was performed on a gas chromatograph 7820A (Agilent Technologies, USA) equipped with a flame ionization detector (GC-FID) and DB-EUPAH capillary column (30 m

length, 0.25 mm internal diameter, 0.25 μm film thickness). The temperatures of the injector and detector were kept at 250°C and 300°C, respectively. The column temperature program ran from 50 to 280°C. After holding the oven temperature at 50°C for the first 2 min the temperature was increased to 160°C at a rate of 1.5°C min^{-1}, then to 230°C at a rate of 6°C min^{-1}, and then to 280°C at a heating rate of 8°C min^{-1} and before it was hold for another 5 min. Nitrogen was used as a carrier gas with a constant flow rate of 1 ml min^{-1}. Data acquisition and processing were performed using Agilent OpenLAB CDS EZChrom A.02.02 (Agilent Technologies, USA). Certain species were calibrated at four levels with solutions of known concentration and 5 replicates per level. Prior to the quantitative analyses in GC-FID, the tar compounds were annotated using a dual detector system GC-MS 5975C TAD Series / GC-FID 7890A (Agilent Technologies, USA). The column temperature and carrier gas settings were kept the same as those used in GC-FID analysis. The mass spectrometer with a quadrapolar type analyzer scanned the range from m/z 35 to m/z 250 resulting in a scan rate of 6.22 scans s^{-1}. The mass spectrometer was operated at unit mass resolution. A 0.5 μl of sample was injected at a 4:1 split ratio. The collected spectra were exported from Chemstation E.02.00.493 (Agilent Technologies, USA) to NetCDF and further processed by the statistical software "R" 2.15.2 [32] that can acquire and align the data, correct baseline, set time-window and perform multivariate analysis [33]. The multivariate analysis using MCR-AR algorithm yielded deconvoluted mass spectra with the well-resolved overlapping peaks [34], which were imported into the mass spectra library software NIST MS Search 2.0 [35]. The area of peaks was normalized to 100 % within

each sample and the mean of triplicate measurements was calculated. The peaks with mass spectra similarity higher than 80 % were used in the tar quantification. The relative response factors (RRFs) were determined for each compound in tar samples using MatLab (version 8.6, MathWorks Inc.).

2.4. Multivariate data analysis

Prior to multivariate analysis, the resulting intensities of all tar compounds were normalized to the intensity of the internal standard. Multivariate analysis was carried out using the SIMCA software (Umetrics AB, version 14.0) to access the effects of different lignocellulosic compounds and residence time using 0.72 m- and 1.06 m-long reactor tube on the composition of tar samples, which were grouped in carbon dioxide, aliphatic hydrocarbons and their derivatives (paraffins, olefins, acetylene, alkanenitriles, cycloolefins), aromatic hydrocarbons (toluene, benzene, ethylbenzene, styrene, etc.), aromatic nitrogen-containing hydrocarbons, triophenes, oxygenates (ester, alcohol, aldehyde), furans, naphthalenes, polyaromatic hydrocarbons, and unknown species. Orthogonal Projections to Latent Structures Discriminant Analysis (OPLS-DA) is a development of partial least squares (PLS) with the aim to increase the interpretability of models by separating the variation that is related to the response from the variation that is unrelated to the response. Using the same settings, the prediction properties are the same for PLS and OPLS [36]. Both methods involve the construction of a regression model maximizing the covariance between the descriptor variables (X) and the response, i.e. the dependent variable, y. Additionally, OPLS performs a filtering step, which captures structured variation not related to the response but overlapping with the related variation, in one or more orthogonal compo-

nents. The loadings of the descriptor variables on those components indicate the origin of the uncorrelated, also called orthogonal, variation. The variation correlated with the response can be interpreted by the loadings on the predictive component of the OPLS model. OPLS-DA has been largely used in the -omics context, and it is now the multivariate linear model of choice for classification/discrimination [37, 38]. The term classification is used when the objective is to classify new objects into one of two or more possible classes (e.g. cellulose, hemicellulose, softwood lignin, wheat straw lignin). The term discrimination is used for the two-class case, in which the objective is to separate two classes and investigate the causes for class separation. In OPLS the vector y is a continuous variable; in two-class discrimination, OPLS-DA y is categorical and, thus, defined as a dummy vector of 0/1 for the two-class case (for the multiple-y case, it is a dummy matrix with a 0/1 vector per class), describing class belonging. R^2X values of the predictive and orthogonal components are measures of the structured fraction of the original data variation describing the response and the fraction not correlated with the response. The quality of an OPLS-DA model is described by the R^2Y value, i.e. the correlation between the observed and predicted values for the studied response, and the Q^2 value, i.e. the correlation between the observed and cross-validated predicted response. The higher the R^2Y and Q^2 value the better the response can be described and predicted as a function of the descriptor variables, respectively. The R^2X, R^2Y, and Q^2 values are normalized to have an upper limit of 1. The low end is around 0 but the results of the cross validation may cause Q^2 to be negative when no model is found [39]. The confidence level was set at 95 %. The model accuracy is evaluated by the

goodness of fit (R^2Y) for the X matrix and goodness of prediction by cross validation (Q^2) [40]. Both R^2Y and Q^2 parameters vary in the range from 0 to 1, with the upper limit of 1 for a perfect fit and 0.5 for an acceptable fit [41]. The number of components in all models was chosen using the autofit approach in SIMCA software that maximizes the relevant Q^2 statistics, while ensuring that all calculated components are significant and stable to resampling. The output of OPLS-DA model was visualized using both score scatter and loading plots. Each point in the score scatter plot represents a tar sample from pyrolysis of cellulose, hemicellulose, softwood lignin and wheat straw lignin using 0.72 m-long or 1.06 m-long reactor tube. Each column in the loading plot corresponds to a GC-MS peak colored according to its identified class of chemical structure.

3. Results and discussion

3.1. Lignin characterization

The effect of lignin type on the organic matter transformation, which affects product yields in high-temperature pyrolysis, was investigated, using ^{13}C CP/MAS and ^{13}C SP/MAS NMR. In the ^{13}C CP/MAS experiments the resonances of the carbons in immobile regions of the samples were enhanced by polarization transfer from the highly abundant ^{1}H nuclei via hetero-nuclear dipolar coupling.

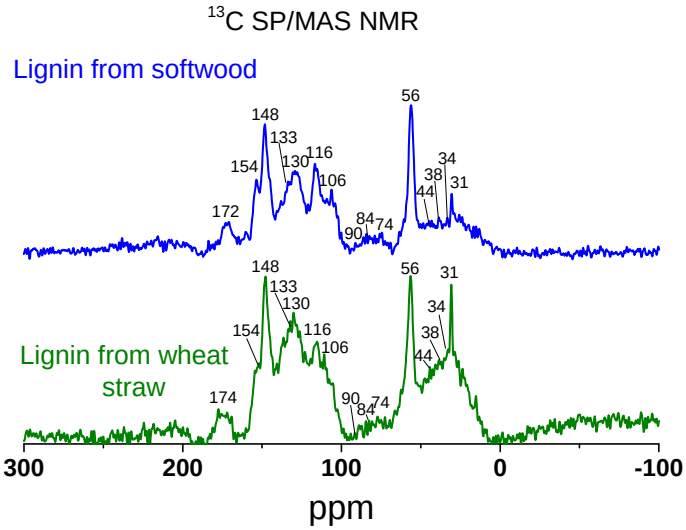

1(a): ^{13}C CP/MAS NMR)

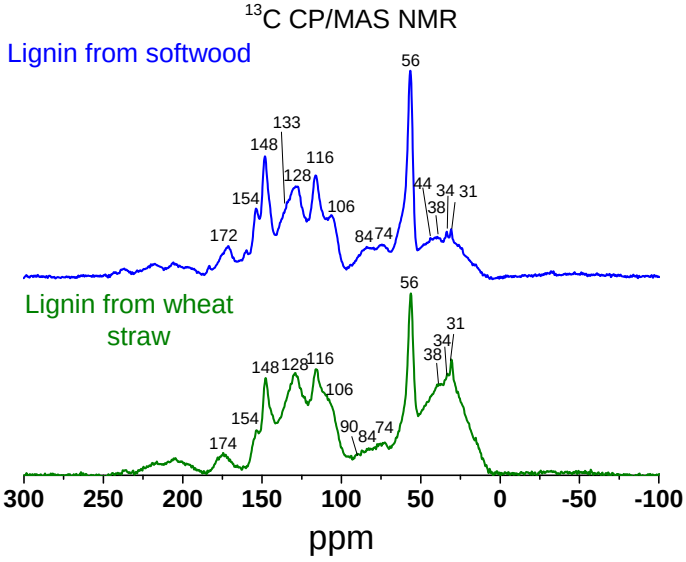

1(b): ^{13}C SP/MAS NMR

Figure 1: ^{13}C CP/MAS and ^{13}C SP/MAS spectra of lignin from softwood and lignin from wheat straw.

All carbon sites were observed quantitatively by the ^{13}C SP/MAS NMR measurements. In Figure 1, the ^{13}C CP/MAS and ^{13}C SP/MAS NMR spectra of lignin from softwood and lignin from wheat straw are displayed, and an assignment of resonances is shown in Table 2.

Table 2: Resonance assignment of ^{13}C CP/MAS and ^{13}C SP/MAS NMR spectra of lignin from softwood and lignin from wheat straw [42–46].

Chemical shift, ppm	**Description**
172-174	Carbohydrate; -COO-R, CH_3-COO-
153-154	Lignin; S3(e), S5(e)
145-148	Lignin; S3(ne), S5(ne), G1(e), G4(e)
133-138	Lignin; S1(e), S4(e), G1(e)
121-130	Lignin; G6
105-116	Carbohydrates; C1, Lignin; S2, S6, G5, G6
89-92	C4 in cellulose (cr)
84-85	C4 in cellulose (am)
72-75	C2, C3 in carbohydrates; C5 in cellulose
56-57	Lignin, OCH_3
30-38	CH_2 in aliphatics

Abbreviations: S, syringyl; G, guaiacyl; ne, in non-etherified arylglycerol β-aryl ethers; e, in etherified arylglycerol β-aryl ethers.

The ^{13}C CP/MAS and ^{13}C SP/MAS NMR spectra of both lignin types are almost identical. The primary difference in the structure of both lignins was in the signal at 31 ppm (methyl group in aliphatic chains) and 106 ppm. According to the specifications of the producer, both organosolv lignin samples contained $< 6\,\%$ residual carbohydrates. The resonances in a range of 72-92 ppm and 106 ppm are most likely due to overlapping resonances from C1-C4 in cellulose and aromatic carbons in lignin. The signal at 106 ppm was more recognizable in NMR spectra of lignin from softwood probably due to

253 the greater fraction of carbohydrates remaining in the lignin after organosolv
254 treatment. The more visible signal at 31 ppm was associated with the pres-
255 ence of p-hydroxyphenol unit in lignin from wheat straw [47]. Comparison
256 of the peak intensities in the region 84-90 ppm of organosolv lignin indicates
257 that the cellulose content in organosolv lignin is low compared to Protobind
258 lignins [48]. Figure 2 shows the IR spectra of lignin from softwood and lignin
259 from wheat straw.

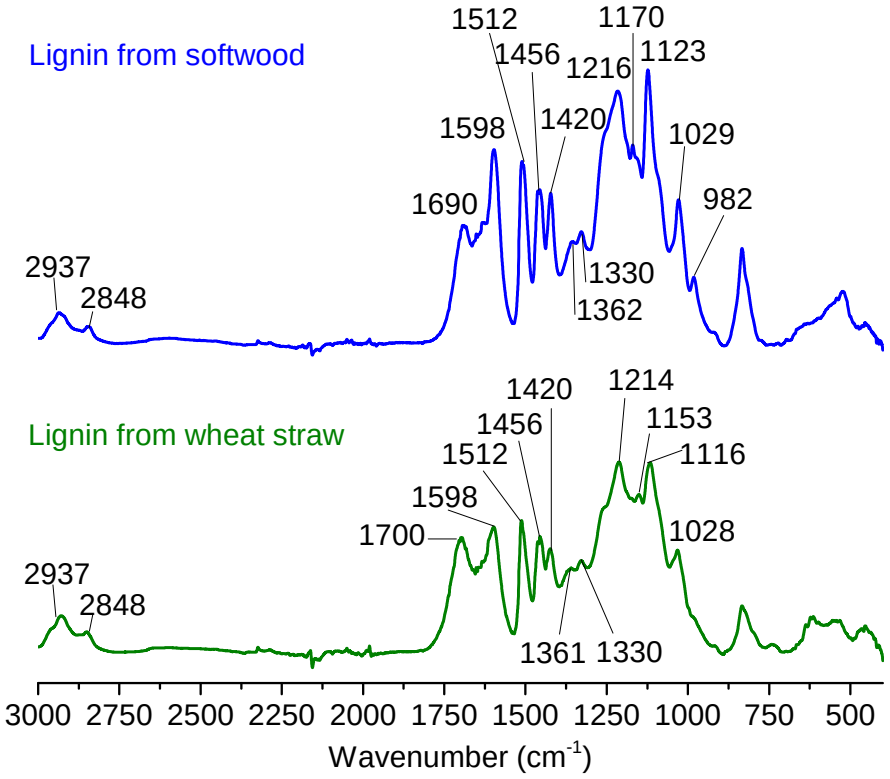

Figure 2: Experimental IR spectra of lignin from softwood and lignin from wheat straw.

260 The assignment of species to each IR band is shown in supplemental ma-

terial (Table S-2) using literature data [49–54]. A strong signal was observed for the lignin from softwood at 1598 and 1512 cm^{-1} which were assigned to the C=C group stretching and suggesting the higher content of aromatic groups than in the lignin from wheat straw. The organosolv process results in cleavage of the β-O-4-linkages which generate both phenolic hydroxyl (1365 cm^{-1}) and carbonyl groups (1700 cm^{-1}) [55]. Both lignin samples were characterized as guaiacyl-syringyl GS type, confirming previous results of Labidi et al. [56]. Moreover, the whole C=O range between 1800-1633 cm^{-1} is intense. Because the C=O vibrations also cause a band around 1270 cm^{-1}, the absorbance here is higher for the lignin from wheat straw than in the case of GS spectra of lignin from softwood [50]. A small band around 1170 cm^{-1} (C=O vibration of esters) is additionally present in the lignin from softwood that is typically to find in the GS lignin type. The IR results indicated that the organosolv process has no significant influence on the lignin structure.

3.2. Identification of tar compounds

The identification of individual tar compounds from GC-MS analysis was confirmed further in comparison with the reference chromatograms of external standards and literature results [10, 57–61]. The identified tar compounds with the relevant information were listed in Table 3. Forty five compounds in the pyrolysis tar have been quantified and grouped for the further modeling using SIMCA.

Table 3: List of identified tar compounds with the empirical formula, molecular weight, retention time and compound category.

No	**Compounds**	**Formula**	**MW**	**RT**	**Cat. name**
				min	
1	Acetonitrile	C_2H_3N	41.05	6.18	AH
2	Benzene	C_6H_6	78.11	6.30	A
3	Toluene	C_7H_8	92.14	9.05	A
4	2-Methylthiophene	C_5H_6S	98.17	9.89	T
5	3-Methylthiophene	C_5H_6S	98.17	10.29	T
6	Pyrrole	C_4H_4NH	67.09	10.74	AN
7	Ethylbenzene	C_8H_{10}	106.17	15.90	SA
8	Styrene	C_8H_8	104.15	17.35	SA
9	1,2,4-Trimethylbenzene	C_9H_{12}	120.19	23.00	SA
10	α-Methylstyrene	C_9H_{10}	118.18	23.70	SA
11	Dimethyl Malonate	$C_5H_8O_4$	132.12	24.27	SA
12	1,2,3-Trimethylbenzene	C_9H_{12}	120.19	26.38	SA
13	Phenol	C_6H_5OH	94.11	26.46	P
14	Benzaldehyde	C_7H_6O	106.12	26.86	O
15	2-Methylphenol	C_7H_8O	108.14	32.87	P
16	1-Phenyl-1-propyne	C_9H_8	116.16	33.56	SA
17	3-Methylphenol	C_7H_8O	108.14	34.81	P
18	Phenyl acetate	$C_8H_8O_2$	136.1	35.13	O
19	3-Methylbenzofuran	C_9H_8O	132.16	37.35	F
20	2-Methylbenzofuran	C_9H_8O	132.16	37.60	F
21	2,6-Dimethylphenol	$C_8H_{10}O$	122.17	38.12	P
22	Naphthalene	$C_{10}H_8$	128.17	46.85	N
23	4-Vinylphenol	C_8H_8O	120.15	49.84	P
24	Quinoline	C_9H_7N	129.16	55.08	AN
25	1-Methylnaphthalene	$C_{11}H_{10}$	142.2	58.44	SN
26	1-Indanone	C_9H_8O	132.16	60.61	SA
27	Indole	C_8H_7N	117.15	62.11	AN
28	Biphenyl	$C_{12}H_{10}$	154.21	64.78	PAH
29	2,6-Dimethylnaphthalene	$C_{12}H_{12}$	156.22	64.98	SN
30	1,3-Dimethylnaphthalene	$C_{12}H_{12}$	156.22	67.01	SN
31	Biphenylene	$C_{12}H_8$	152.19	71.55	PAH
32	Acenaphthene	$C_{12}H_{10}$	154.2	75.02	PAH

No	Compounds	Formula	MW	RT	Cat. name
33	Dibenzofuran	$C_{12}H_8O$	168.19	77.01	F
34	Fluorene	$C_{13}H_{10}$	166.22	80.70	PAH
35	2-Methylfluorene	$C_{14}H_{12}$	180.25	84.62	PAH
36	4-Methylfluorene	$C_{14}H_{12}$	180.25	85.48	PAH
37	Phenanthrene	$C_{14}H_{10}$	178.23	88.05	PAH
38	Anthracene	$C_{14}H_{10}$	178.23	88.22	PAH
40	1-Methylphenanthrene	$C_{15}H_{11}$	192.26	90.98	PAH
41	4H-Cyclopenta[def]phenanthrene	$C_{15}H_{10}$	190.25	91.08	PAH
42	2-Phenylnaphthalene	$C_{16}H_{12}$	204.27	91.64	PAH
43	Fluoranthene	$C_{16}H_{10}$	202.26	92.09	PAH
44	Pyrene	$C_{16}H_{10}$	202.25	92.99	PAH
45	2-Methylpyrene	$C_{17}H_{12}$	216.28	97.59	PAH

A: Aromatic compounds

AH: Aliphatic hydrocarbons

AN: Aromatic nitrogen-containing compounds

F: Furans

N: Naphthalenes

O: Oxygenates

PAH: Polyaromatic compounds

P: Phenols

SA: Substituted aromatic compounds

SN: Substituted naphthalenes

T: Triophenes

3.3. Tar and soot yields

Figure 3 shows the change in the yields of tar from pyrolysis of cellulose, hemicellulose, lignin from softwood, lignin from wheat straw, and KNO_3 doped lignin from wheat straw in the range from 800 to 1250°C at three particle residence times. The pyrolysis of lignin gave a greater tar yield compared to pyrolysis of cellulose and hemicellulose. The differences in the tar yield from pyrolysis of lignin from softwood and lignin from wheat straw were small.

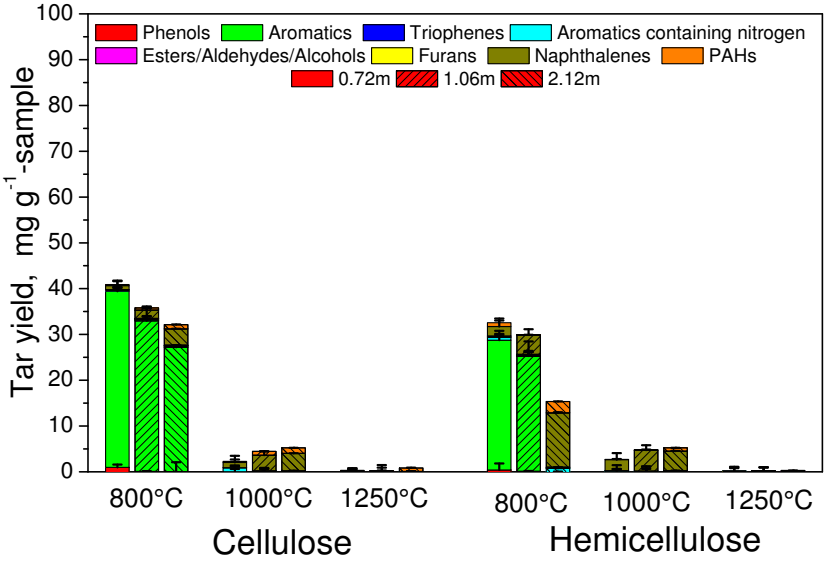

3(a): Cellulose and Hemicellulose

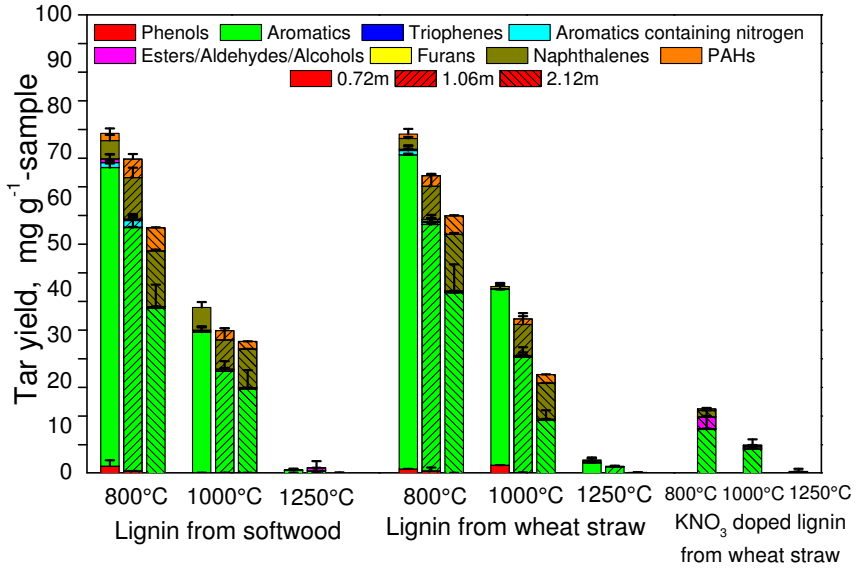

3(b): Lignin

Figure 3: Tar yields (mg g^{-1} on dry basis) of cellulose, hemicellulose, lignin from softwood, lignin from wheat straw, and KNO_3 doped lignin from wheat straw.

In general, the yield of identified tar decreased with the increased heat treatment temperature and with the increased residence time. The addition of alkali nitrates to the lignin from wheat straw led to the decrease in tar yields. The high level of alkali metals in biocarbon catalyzes the conversion of bridges into char, promoting faster devolatilization rates and surpressing tar formation, leading to greater char yields [62, 63]. The yields of phenols and aromatic compounds decreased and the yields of naphthalene and PAHs increased with an increase in heat treatment temperature from 800 to 1000°C in pyrolysis of all lignocellulosic compounds. More esters, aldehydes and alcohols were formed with the addition of alkali nitrates to lignin from wheat straw at 800°C due to the function of alkali metals to break the aromatic rings [64]. Figure 4 illustrates that the soot yields from pyrolysis of lignocellulosic compounds was the greatest at 1250°C, whereas the formation of tars was the lowest under similar operating conditions. The greatest soot yield (daf) was obtained from pyrolysis of lignin due to the stronger formation of PAH precursors. The conversion of tars to the light aromatic compounds could contribute to the greater soot yields with the longer residence time and increased heat treatment temperature. The results showed that significantly less soot was formed during pyrolysis of cellulose and hemicellulose due to the lower fraction of phenolic groups. The formation of soot was not affected by the differences in lignin composition. During pyrolysis of KNO_3 doped lignin from wheat straw, the soot and tar yields decreased with the increased heat treatment temperature.

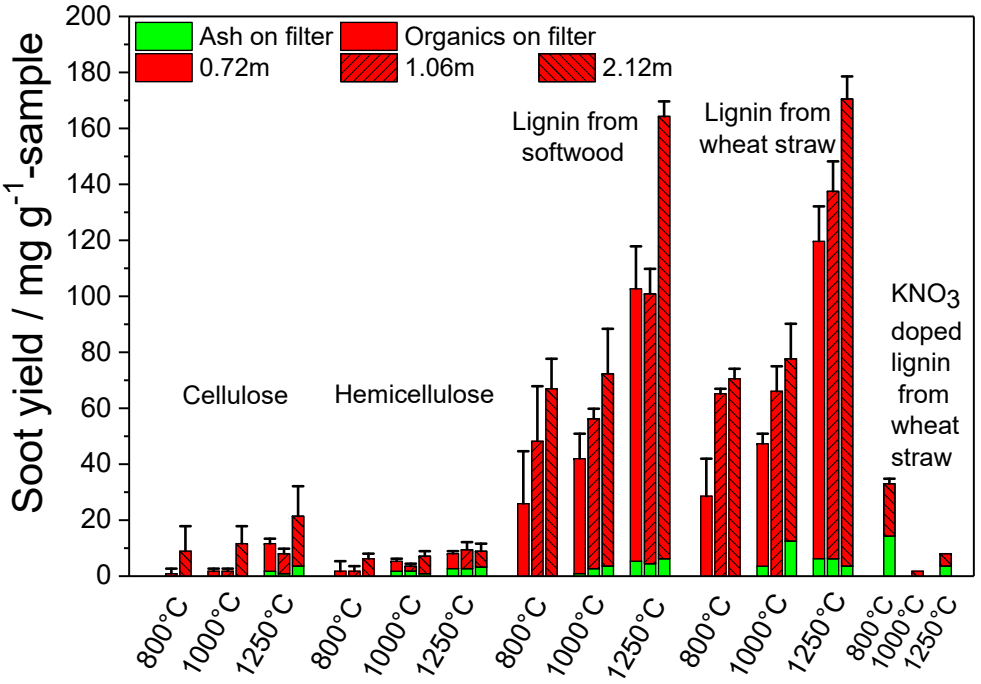

Figure 4: Soot yields (mg g^{-1} on dry basis) of cellulose, hemicellulose, lignin from softwood, lignin from wheat straw, and KNO_3 doped lignin from wheat straw.

3.4. Modeling of tar yields and composition

The OPLS-DA score scatter plot in Figure 5 shows that tar samples from pyrolysis of cellulose, hemicellulose, softwood lignin and wheat straw lignin using 0.72 m- and 1.06 m-long reactor tube were well separated into two clusters. The majority of variables related to tar samples generated in 0.72 m-long reactor tube appeared in two left quadrants, whereas the majority of tar samples from pyrolysis in 1.06 m-long tube reactor was plotted in two right quadrants in the score scatter plot. This indicated a good separation of model compounds and emphasized the importance of residence time on the

322 tar composition.

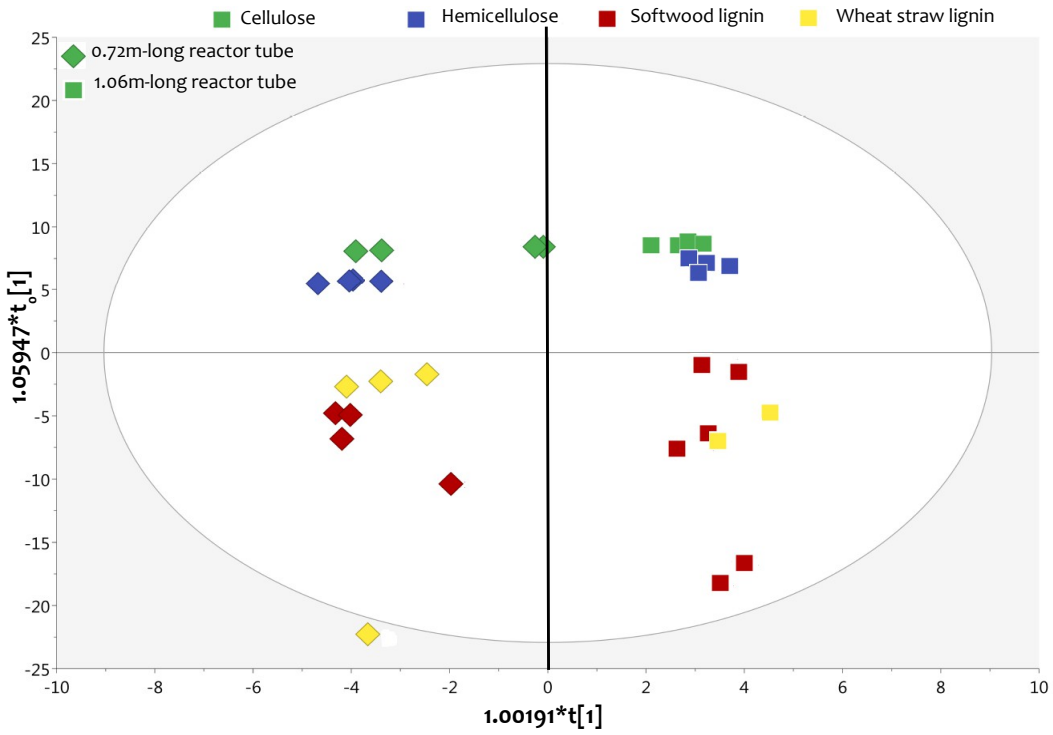

Figure 5: The OPLS-DA score scatter plot ($R^2Y = 0.91$, $Q^2 = 0.85$) displays the clustering of tar samples from pyrolysis of cellulose, hemicellulose, softwood lignin and wheat straw lignin using 0.72 m- and 1.06 m-long reactor tube. Tar samples produced at the same residence time appear to group together. The tar composition of both lignin samples is significantly different from the tar composition of holocelluloses at both residence times.

323 The OPLS-DA column loading plot in Figure 6 confirms that the resi-
324 dence time has a strong influence on the tar composition. Single ring com-
325 pounds such as aliphatic hydrocarbons, phenols, aromatics, oxygenates were
326 more abundant in pyrolysis using 0.72 m-long reactor tube. The 2-4 ring

polyaromatic hydrocarbons (PAHs) and nitrogen-containing aromatics were mostly formed in pyrolysis using 1.06 m-long reactor tube, confirming previous results of Onwudili et al. [65]. The low concentrations of large PAH with aliphatic chains might be related to the formation of more stable products or soot with increasing residence time [66]. The aromatics with attached aliphatic chains show significantly higher nucleation rates than the polycyclic aromatic hydrocarbons of similar mass without any chain [67]. The concentrations of benzene and toluene which belong to dominating compounds in tar samples from all lignocellulosic compounds remained unchanged, while the amount of triophenes was similarly small with increasing residence time. The yield of phenanthrene exhibited an order of magnitude higher concentration than anthracene, while the concentrations of phenanthrene and anthracene were almost twice as low as that of naphthalene and its derivatives, confirming the previous results of Kislov et al. [68]. The OPLS-DA column loading plot 6 shows that a small fraction of naphthalene molecules which were not converted to larger PAHs, formed substituted structures with one or two ethyl or methyl groups with increasing residence time. Numerous nitrogen-containing aromatic compounds were formed at long residence time. The OPLS-DA score scatter plot in Figure 5 shows that tar samples from cellulose and hemicellulose pyrolysis appeared to group tightly together in the upper quadrants, whereas both lignin tar samples were clustered in the lower quadrants. This demonstrated significant differences in tar composition among holocelluloses and lignin. The dominating products derived from pyrolysis of softwood lignin were phenols, aromatic compounds, naphthalenes and PAHs, whereas the oxygenates were mostly present in tar samples from hemicellu-

lose pyrolysis (supplementary Figures S-6 and S-7).

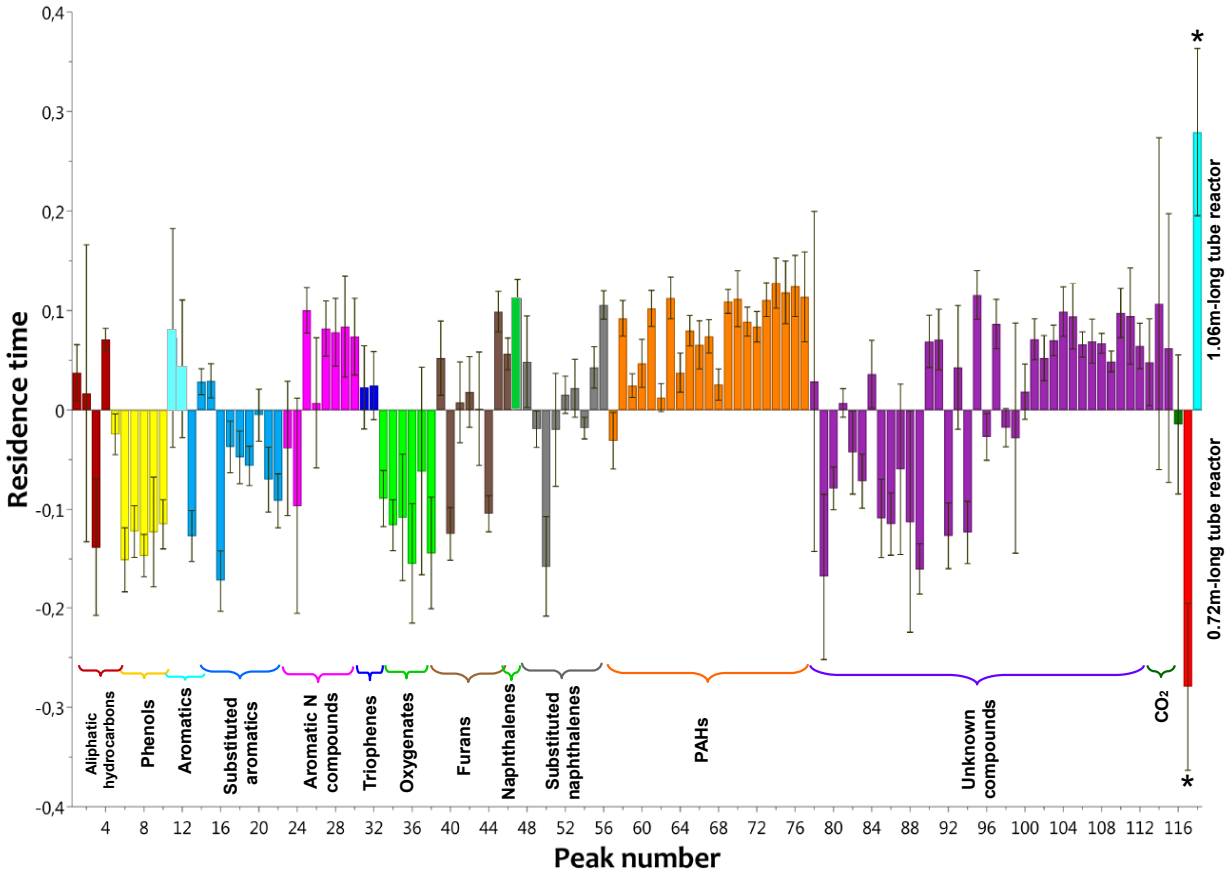

Figure 6: The OPLS-DA column loading plot ($R^2Y = 0.91$, $Q^2 = 0.85$) visualizes differences in the composition of tar samples generated in pyrolysis using 0.72 m- and 1.06 m-long reactor tube. The value of variables pointing in the same direction as columns of tar compounds from pyrolysis using 0.72 m-long reactor tube is higher in that group than the value of variables pointing in the opposite direction. The higher the column and smaller the error bar, the greater the contribution of the variable to the model [69]. Error bars denote the 95 % confidence level.

The tar composition within the lignocellulosic compound class (holo-

celluloses or lignin) remained nearly similar, as shown in the supplemental material (Figures S-3, S-5, S-6 and S-7). More phenols, aromatic compounds, triophenes, furans, naphthalenes, substituted naphthalenes, substituted aromatics and PAHs were observed in hemicellulose tars than in products from cellulose pyrolysis due to the lignin-associated impurities in hemicelluloses (supplementary Figure S-3). Interestingly, the cellulose tars contained the high concentration of acetic acids which were probably formed from the decomposition of 5-hydroxymethylfurfural [70].

The present OPLS-DA model ($R^2Y = 0.91$, $Q^2 = 0.85$) can explain most of the variations within the data set and can predict well the sediment age from the GC-MS data set. The OPLS-DA model for tar samples from softwood lignin and wheat straw lignin explained 61 % of variation in the tar composition, but was less reliable ($Q^2 = 0.21$) than the OPLS-DA models for cellulose/hemicellulose ($R^2Y = 0.97$, $Q^2 = 0.99$) and hemicellulose/softwood lignin tar compounds ($R^2Y = 0.89$, $Q^2 = 0.87$). The prediction of the model for tar samples from softwood lignin and wheat straw lignin was mostly affected by the systematic errors associated with the tar collection and storage [71]. Further progress in the prediction of tar composition can be advanced by improvement in the accuracy of experimental measurements, as well as prediction of tar composition using other advanced techniques. The results showed that the precision of the lignin tar model can not be improved by the variation of predictive and orthogonal components.

4. Conclusion

This work presents yields and composition of tars for lignocellulosic compounds reacted in a drop-tube furnace operating in the temperature range from 800 to 1250°C. The present results indicate that the dominating products in tars from pyrolysis of all lignocellulosic compounds were aromatics. The minor differences in a tar composition were in a greater fractions of oxygenates in holocellulose pyrolysis, whereas more phenols, PAHs and naphthalene were observed in the lignin pyrolysis. No significant differences were observed in the yield and composition of lignin from softwood and lignin from wheat straw despite greater aromatic content in lignin from softwood. Longer residence time and higher heat treatment temperatures led to the decrease in tar yields and greater soot formation. Simultaneous reduction of tar and soot was achieved by impregnation of lignin from wheat straw with aqueous KNO_3 solution, leading to reduction of light hydrocarbons. The present OPLS-DA model can explain most of the variations within the experimental GC-MS data set by showing that the moisture, oxygen and carbon content in the original feedstock has more influence on the tar compositional differences among the lignocellulosic compounds than the inorganic content with less than 4.3 % in the original feedstock.

Acknowledgements

The authors gratefully acknowledge financial support from the Kempe Foundations and the Swedish strategic research program Bio4Energy. We are grateful to the plant cell wall and carbohydrate analytical facility at UPSC/SLU, supported by Bio4Energy and TC4F for the GC-MS analysis.

The authors acknowledge the facilities and technical support of Dr. Junko Takahashi-Schmidt at Umeå Plant Science Centre. Dr. Flemming Hofmann Larsen and Dr. Soren Talbro Barsberg at University of Copenhagen are acknowledged for the technical support with NMR and FTIR analysis. We acknowledge Raymond Mclnerney from University of Limerick for the article proof-reading.

References

[1] Serrano-Ruiz JC, Dumesic JA, Catalytic routes for the conversion of biomass into liquid hydrocarbon transportation fuels, Energy Environ Sci 4 (1) (2010) 83–99.

[2] Puig-Arnavat M, Soprani S, Søgaard M, Engelbrecht K, Ahrenfeldt J, Henriksen UB, Hendriksen PV, Integration of mixed conducting membranes in an oxygen-steam biomass gasification process, RSC Adv 3 (2013) 20843–54.

[3] Kinoshita CM, Wang Y, Zhou J, Tar formation under different biomass gasification conditions, J Anal Appl Pyrolysis 29 (1994) 169–81.

[4] Di Blasi C, Modeling chemical and physical processes of wood and biomass pyrolysis, Prog Energy Combust Sci 34 (2008) 47–90.

[5] Umeki K, Yamamoto K, Namioka T, Yoshikawa K, High temperature steam-only gasification of woody biomass, Appl Energy 87 (2010) 791–8.

[6] Font-Palma C, Model for biomass gasification including tar formation and evolution, Energy Fuels 27 (2013) 2693–702.

[7] Fuentes-Cano D, Gomez-Barea A, Nilsson S, Generation and secondary conversion of volatiles during devolatilization of dried sewage sludge in a fluidized bed, Ind End Chem Res 52 (2013) 1234–43.

[8] Nik-Azar M, Hajaligol MR, Sohrabi M, Dabir B, Effects of heating rate and particle size on the products yields from rapid pyrolysis beechwood, Fuel Sci Tech Int 14 (4) (1996) 479–502.

[9] Milne TA, Abatzoglou N, Evans RJ, Biomass Gasifier "Tars". Their Nature, Formation and Conversion Golden (CO): National Renewable Energy Laboratory; 1998 November Report No. NREL/TP-570-25357. Contract No.: DE-AC36-83-CH10093 .

[10] Evans RJ, Milne TA, Molecular characterization of the pyrolysis of biomass, Energy Fuels 1 (1987) 123–37.

[11] Evans RJ, Milne TA, Molecular characterization of the pyrolysis of biomass.II. Fundamentals, Energy Fuels 1 (4) (1987) 311–9.

[12] Wolfesberger-Schwabl U, Aigner I, Hofbauer H, Mechanism of Tar Generation during Fluidized Bed Gasification and Low Temperature Pyrolysis, Ind Eng Chem Res 51 (2012) 13001–7.

[13] Wang H, Frenklach A, A detailed kinetic modeling study of aromatics formation in laminar premixed acetylene and ethylene flames, Combust Flame 110 (1997) 173–221.

[14] Jarvis MW, Haas TJ, Donohoe BS, Daily JW, Gaston KR, Frederick WJ, Elucidation of biomass pyrolysis products using a laminar entrained flow reactor and char particle imaging, Fuel 25 (2011) 324–36.

[15] Morf P, Hasler P, Nussbaumer T, Mechanisms and kinetics of homogeneous secondary reactions of tar from continuous pyrolysis of wood chips, Fuel 81 (2002) 843–53.

[16] Fuentes-Cano D, Gomez-Barea A, Nilsson S, Ollero P, Kinetic modeling of tar and light hydrocarbons during the thermal conversion of biomass, Energy Fuels 30 (2016) 377–85.

[17] Jess A, Mechanisms and kinetics of thermal reactions of aromatic hydrocarbons from pyrolysis of solid fuels, Fuel 75 (1996) 1441–8.

[18] Fraga AR, Gaines AF, Kandiyoti R, Characterization of biomass pyrolysis tars produced in the relative absence of extraparticle secondary reactions, Fuel 70 (7) (1991) 803–9.

[19] Hajaligol MR, Howard JB, Peters WA, An Experimental and Modeling Study of Pressure Effects on Tar Release by Rapid Pyrolysis of Cellulose Sheets in a Screen Heater, Combust Flame 95 (1993) 47–60.

[20] Nik-Azar M, Hajaligol MR, Sohrabi M, Dabir B, Mineral matter effects in rapid pyrolysis of beechwood, Fuel Process Tech 51 (1997) 7–17.

[21] Hoekstra E, Van Swaaij WPM, Kersten SRA, Hogendoorn KJA, Fast pyrolysis in anovel wire-mesh reactor: Decomposition of pine wood and model compounds, Chem Eng J 187 (2012) 172–84.

[22] Bach-Oller A, Kirtania K, Furusjö E, Umeki K, Co-gasification of black liquor and pyrolysis oil at high temperature: Part 2. Fuel conversion, Fuel 197 (2017) 240–7.

[23] Qin K, Lin W, Fœster S, Jensen PA, Wu H, Jensen AD, Characterization of Residual Particulates from Biomass Entrained Flow Gasification, Energy Fuels 27 (1) (2013) 262–70.

[24] Septien S, Valin S, Peyrot M, Dupont C, Salvador S, Characterization of char and soot from millimetric wood particles pyrolysis in a drop tube reactor between 800°C and 1400°C, Fuel 121 (2014) 216–24.

[25] Trubetskaya A, Jensen PA, Jensen AD, Garcia Llamas AD, Umeki K, Gardini D, Kling J, Bates RB, Glarborg P, Effects of several types of biomass fuels on the yield, nanostructure and reactivity of soot from fast pyrolysis at high temperatures, Appl Energy 171 (2016) 468–82.

[26] Trubetskaya A, Jensen PA, Jensen AD, Garcia Llamas AD, Umeki K, Glarborg P, Effect of fast pyrolysis conditions on biomass solid residues at high temperatures, Fuel Process Technol 143 (2016) 118–29.

[27] Trubetskaya A, Jensen PA, Jensen AD, Steibel M, Spliethoff H, Glarborg P, Influence of fast pyrolysis conditions on yield and structural transformation of biomass char, Fuel Process Technol 140 (2015) 205–14.

[28] Bouraoui Z, Dupont C, Jeguirim M, Limousy L, Gadiou R, CO_2 gasification of woody biomass chars: The influence of K and Si on char reactivity, C R Chimie (2016) 1–9.

[29] Peersen OB, Wu X, Kustanovich I, Smith SO, Variable-Amplitude Cross-Polarization MAS NMR, J Magn Reson Ser A 104 (1993) 334–9.

[30] Bennett AE, Rienstra CM, Auger M, Lakshmi KV, Griffin RG, Heteronuclear decoupling in rotating solids, J Chem Phys 103 (16) (1995) 6951–8.

[31] Barsberg S, Thygesen LG, Sanadi AR, Control of Lignin Solubility and Particle Formation Modulates its Antioxidant Efficiency in Lipid Medium: An In Situ Attenuated Total Reflectance FT-IR Study, Environ Sci Technol 28 (2014) 4539–44.

[32] R-Development-Core-Team, R: A Language and Environment for Statistical Computing, http://www.R-project.org/ .

[33] Tolu J, Gerber L, Boily JF, Bindler R, High-throughput characterization of sediment organic matter by pyrolysis-gas chromatography/mass spectrometry and multivariate curve resolution: A promising analytical tool in (paleo)limnology, Anal Chim Acta 880 (2015) 93–102.

[34] Gerber L, Eliasson M, Trygg J, Moritz T, Sundberg B, Multivariate curve resolution provides a high-throughput data processing pipeline for pyrolysis-gas chromatography/mass spectrometry, J Anal Appl Pyrolysis 95 (2012) 95–100.

[35] MS-SEARCH, NIST Mass Spectrometry Data Center: NIST/EPA/NIH Mass Spectral Database, http://chemdata.nist.gov .

[36] Trygg J, Wold S, Orthogonal projections to latent structures (O-PLS), J Chemom 16 (3) (2002) 119–28.

[37] Bylesjö M, Rantalainen M, Cloarec O, Nicholson JK, Holmes E, Trygg J, OPLS discriminant analysis: combining the strengths of PLS-DA and SIMCA classification, J Chemom 20 (8-10) (2006) 341–51.

[38] Yap IK, Brown IJ, Chan Q, Wijeyesekera A, Garcia-Perez I, Bictash M and etc., Metabolome-wide association study identifies multiple biomarkers that discriminate north and south Chinese populations at differing risks of cardiovascular disease: INTERMAP study, J Proteome Res 9 (12) (2010) 6647–54.

[39] Souihi N, Dumarey M, Wikström H, Tajarobi P, Fransson M, Svensson O and etc., A quality by design approach to investigate the effect of mannitol and dicalcium phosphate qualities on roll compaction, Int J Pharma 447 (2013) 47–61.

[40] Strandberg A, Holmgren P, Broström M, Predicting fuel properties of biomass using thermogravimetry and multivariate data analysis, Fuel Process Tech 156 (2017) 107–12.

[41] Blasco H, Blaszczynski J, Billaut JC, Nadal-Desbarats L, Pradat PF, Devos D and etc., Comparative analysis of targeted metabolomics: Dominance-based rough set approach versus orthogonal partial least square-discriminant analysis, J Biotech Inform 53 (2015) 291–9.

[42] Bardet M, Gerbaud G, Giffard M, Doan C, Hediger S, Pape LL, ^{13}C high-resolution solid-state NMR for structural elucidation of archaeological woods, Prog Nucl Magn Reson Spectrosc 55 (3) (2009) 199–214.

[43] Bardet M, Maron S, Foray MF, Berger M, Guillermo A, Investigation of gamma-Irradiated Vegetable Seeds with High-Resolution Solid-State ^{13}C NMR, Radiat Res 161 (4) (2004) 458–63.

[44] Xu F, Sun JX, Sun R, Fowler P, Baird M, Comparative study of organosolv lignins from wheat straw, Ind Crops Products 23 (2006) 180–93.

[45] Webster EA, Chudek JA, Hopkins DW, Carbon transformations during decomposition of different components of plant leaves in soil, Soil Biol Biochem 32 (3) (2000) 301–14.

[46] Reid DG, Bonnet SL, Kemp G, van der Westhuizen JH, Analysis of commercial proanthocyanidins. Part 4: Solid state ^{13}C NMR as a tool for in situ analysis of proanthocyanidin tannins, in heartwood and bark of quebracho and acacia, and related species, Photochem 94 (2013) 243–8.

[47] Ghaffar SH, Fan M, Structural analysis for lignin characteristics in biomass straw, Biomass Bioenergy 57 (2013) 264–79.

[48] Cabrera Y, Cabrera A, Hofmann Larsen F, Felby C, Solid state ^{29}Si NMR and FTIR analyses of lignin-silica coprecipitates, Holzforschung 70 (8) (2016) 709–18.

[49] Sarkanen KV, Chang HM, Ericsoon B, Species variations in lignins. I. Infrared spectra of guaiacyl and syringyl models, Tappi 50 (11) (1967) 572–5.

[50] Faix O, Classification of Lignins from Different Botanical Origins by FT-IR Spectroscopy, Holzforschung (1991) 21–7.

[51] Tejado A, Pena C, Labidi J, Echeverria JM, Mondragon I, Physico-chemical characterization of lignins from different sources for use in phenol-formaldehyde resin synthesis, Biores Tech 98 (2007) 1655–63.

[52] Schultz TP, Glasser WG, Quantitative Structural Analysis of Lignin by Diffuse Reflectance Fourier Transform Infrared Spectrometry, Holzforschung 40 (1986) 37–44.

[53] Popescu CM, Singurel G, Vasile C, Argyropoulos DS, Willfor S, Spectral chracterization of eucalyptus wood, Appl Spect 61 (11) (2007) 1168–77.

[54] Sun SN, Li MF, Yuan TQ, Xu F, Sun RC, Effect of ionic liquid/organic solvent pretreatment on the enzymatic hydrolysis of corncob for bioethanol production. Part 1: Structural characterization of the lignins, Ind Crops Products 43 (2013) 570–7.

[55] Nimz H, Das Lignin der Buche - Entwurd eines Konstitutionsschemas, Angew Chem 86 (9) (1974) 336–44.

[56] dos Santos PSB, de Cademartori PHG, Prado R, Gatto DA, Labidi J, Composition and structure of organosolv lignins from four eucalypt species, Wood Sci Tech 48 (4) (2014) 873–85.

[57] Haanappel VAC, Stevens TW, Hovestad A, Skolnik V, Visser R, Gas chromatographic-mass spectrometric analysis of tar compounds formed during pyrolysis of rice husks, J Chrom 562 (1991) 531–45.

[58] Branca C, Giudicianni P, Di Blasi C, GC/MS Characterization of Liquids Generated from Low-Temperature Pyrolysis of Wood, Ind Eng Chem Res 42 (2003) 3190–202.

[59] Dufour A, Girods P, Masson E, Normand S, Rogaume Y, Zoulalian A, Comparison of two methods of measuring wood pyrolysis tar, J Chrom A 1164 (2007) 240–7.

[60] Wang Z, Li K, Lambert P, Yang C, Identification, characterization and quantitation of pyrogenic polycylic aromatic hydrocarbons and other organic compounds in tire fire products, J Chrom A 1139 (2007) 14–26.

[61] Nowakowski DJ, Bridgwater AV, Elliott DC, Meier D, de Wild P, Lignin fast pyrolysis: Results from an international collaboration, J Anal Appl Pyr 88 (2010) 53–72.

[62] Niksa S, Predicting the rapid devolatilization of diverse forms of biomass with bio-Flashchain, Proc Combust Inst 28 (2) (2000) 2727–33.

[63] Nik-Azar M, Hajaligol MR, Sohrabi M, Dabir B, Mineral matter effects in rapid pyrolysis of beechwood, Fuel Process Technol 51 (1-2) (1997) 7–17.

[64] Bach-Oller A, Alkali-enhanced gasification of biomass: laboratory-scale experimental studies. PhD thesis, Luleå University of Technology, 2018.

[65] Onwudili JA, Insura N, Williams PT, Composition of products from the pyrolysis of polyethylene and polystyrene in a closed batch reactor: Effects of temperature and residence time, J Anal Appl Pyrol 86 (2009) 293–303.

[66] Shukla B, Koshi M, A novel route for PAH growth in HACA based mechanisms, Combust Flame 159 (2012) 3589–96.

601 [67] Chung S, Violi A, Peri-condensed aromatics with aliphatic chains as key
602 intermediates for the nucleation of aromatic hydrocarbons, P Combust
603 Inst 33 (2011) 693–700.

604 [68] Kislov VV, Sadovnikov AI, Mebel AM, Formation Mechanism of Poly-
605 cyclic Aromatic Hydrocarbons beyond the Second Aromatic Ring, J
606 Phys Chem A 117 (2013) 4794–816.

607 [69] Gudmundsdottir J, Oskarsdottir S, Skogberg G, Lindren S, Lundberg V,
608 Berglund M and etc., Early thymectomy leads to premature immuno-
609 logic ageing: An 18-year follow-up, J Allergy Clinical Immunol 138 (5)
610 (2016) 1439–43.

611 [70] Wang S, Guo X, Liang T, Zhou Y, Luo Z, Mechanism research on cellu-
612 lose pyrolysis by Py-GC/MS and subsequent density functional theory
613 studies, Biores Technol 104 (2011) 722–8.

614 [71] Lundell AC, Johansen S, Adlerberth I, Wold AE, Hesselmar B, Rudin
615 A, High Proportion of $CD5^+$ B Cells in Infants Predicts Development
616 of Allergic Disease, J Immun 193 (2) (2014) 510–8.